AGU ADVANCING EARTH AND SPACE SCIENCES

Geophysical Research Letters

RESEARCH LETTER
10.1029/2023GL105389

Anthropogenic Aerosols Contribute to the Recent Decline in Precipitation Over the U.S. Southwest

Yan-Ning Kuo[1], Hanjun Kim[1], and Flavio Lehner[1,2,3]

[1]Department of Earth and Atmospheric Sciences, Cornell University, Ithaca, NY, USA, [2]Climate and Global Dynamics Laboratory, National Center for Atmospheric Research, Boulder, CO, USA, [3]Polar Bears International, Bozeman, MT, USA

Key Points:

- We quantify the role of anthropogenic aerosols in post-1980 Pacific sea surface temperatures and the U.S. Southwest precipitation decline
- Internal variability dominates the winter-spring precipitation trend but aerosols contribute to it through their influence on Pacific SSTs
- Community Earth System Model version 2 simulates a tug-of-war between aerosols and other forcings (e.g., greenhouse gases) and its response to aerosols might be too weak

Supporting Information:

Supporting Information may be found in the online version of this article.

Correspondence to:

Y.-N. Kuo,
yk545@cornell.edu

Citation:

Kuo, Y.-N., Kim, H., & Lehner, F. (2023). Anthropogenic aerosols contribute to the recent decline in precipitation over the U.S. Southwest. *Geophysical Research Letters*, *50*, e2023GL105389. https://doi.org/10.1029/2023GL105389

Received 11 JUL 2023
Accepted 8 NOV 2023

Author Contributions:

Conceptualization: Yan-Ning Kuo, Hanjun Kim, Flavio Lehner
Formal analysis: Yan-Ning Kuo
Funding acquisition: Flavio Lehner
Investigation: Yan-Ning Kuo, Flavio Lehner
Methodology: Yan-Ning Kuo
Resources: Flavio Lehner
Supervision: Flavio Lehner
Visualization: Yan-Ning Kuo
Writing – original draft: Yan-Ning Kuo, Flavio Lehner
Writing – review & editing: Yan-Ning Kuo, Hanjun Kim, Flavio Lehner

Abstract The winter-spring precipitation over the Southwestern United States (SWUS) decreased since 1980. It is frequently attributed to Pacific internal decadal variability, but recent studies found anthropogenic aerosols (AA) can also induce a transition to a negative Pacific Decadal Variability (PDV) phase. We revisit the attribution of SWUS drying by quantifying the contributions of anthropogenically forced decadal Pacific Sea Surface Temperatures (SSTs). Applying a low-frequency component analysis to observations, Community Earth System Model version 2 (CESM2) all-forcings and single-forcing large ensembles, we find up to 42% of the observed precipitation trend to be related to the AA-induced negative PDV-like pattern, which is driven by the emission shift from the Western to the Eastern Hemisphere. In CESM2, other radiative forcings counteract the influence of AA, but it remains unclear whether the model correctly simulates this balance. This implies that the near-future trajectories of these forcings, in particular Asian aerosols, are important for projections of SWUS precipitation.

Plain Language Summary Water resources of the Southwestern United States (SWUS) rely on winter-spring precipitation, which has been declining since 1980. To understand the reasons for the decline, we evaluate the impacts of human-caused Pacific Sea Surface Temperature (SST) changes on SWUS precipitation. We use observations and climate model experiments together with statistical approaches. We find evidence that the shift of aerosol emissions from the Western to the Eastern Hemisphere induced a change in Pacific SSTs that in turn favors a winter-spring SWUS precipitation decline. Additionally, we showed that other human-caused factors, such as greenhouse gases, can offset the impact of aerosols. This means that the near-future SWUS precipitation change depends on the trajectories and the interactions of these various human-caused factors.

1. Introduction

In recent decades, water resources in the Southwestern United States (SWUS) have been strained due to the combination of a prolonged drought (Delworth et al., 2015; Williams et al., 2022) and increasing demand from population growth (Gleick, 2010). This region is particularly vulnerable to climate change, as drought conditions are projected to become more severe with warming (Seager & Hoerling, 2014; Williams et al., 2020). However, projecting future drought risk at regional scales remains challenging (Marvel et al., 2019) because of the existing uncertainty of regional precipitation changes (Polade et al., 2017; Ukkola et al., 2020). Water resources in the SWUS depend critically on winter-spring precipitation, which has been decreasing since 1980. What are the drivers of this decline, and can a better understanding of historical precipitation trends inform precipitation projections?

Winter-spring SWUS precipitation is strongly influenced by internal variability (Seager & Hoerling, 2014), including air-sea coupled modes of variability and internal atmospheric variability (Lehner et al., 2018; Lin et al., 2017; McKinnon & Deser, 2021; Zhang et al., 2021). Teleconnections originating from Pacific sea surface temperature (SST) variability on different time scales (e.g., inter-annually from El Niño-Southern Oscillation, ENSO, or inter-decadally from Pacific decadal variability, PDV) determine a substantial fraction of the variability in SWUS precipitation (Lehner et al., 2018). When the tropical Pacific SSTs are warm (El Niño or positive phase of PDV), anomalous tropical deep convection triggers Rossby waves deepening the Aleutian Low (AL; Horel & Wallace, 1981) and increases the moisture transport into the SWUS (Chavez et al., 2003)—and vice versa. Furthermore, the inter-model spread of future wintertime North Pacific sea level pressure changes is associated with a Pacific Decadal Oscillation (PDO)-like pattern (Choi et al., 2016), implying that North Pacific

ocean-atmosphere coupling is an important source of projection uncertainty for winter-spring SWUS precipitation. However, decadal SST variability might not be purely internal. For example, anthropogenic aerosols (AA) have been reported to induce a negative PDV-like pattern, especially after 1980 (Dittus et al., 2021; Qin et al., 2020; Takahashi & Watanabe, 2016; Wills et al., 2018). To what extent is the PDV-driven SWUS precipitation decline actually an AA-forced response?

Anthropogenically forced SWUS precipitation trends have been reported to be either weak (Delworth et al., 2015; Seager, Osborn, et al., 2019) or lacking model agreement (Pierce et al., 2013; Polade et al., 2017). Often, historical AA forcing counteracts the greenhouse gases (GHGs)-forced response (Deser, Phillips, et al., 2020; Samset, 2018; Zhao et al., 2019), including for Pacific SSTs (Heede & Fedorov, 2021). However, the potential for attributing observed SWUS precipitation trends to AA has received less attention. This is partly due to the challenge of attributing regional aerosol influences directly, given the small signal-to-noise ratio (S/N) in observations and the lack of model agreement (Bonfils et al., 2020). Quantifying the more robust influence of AA on PDV and then inferring associated SST-driven precipitation trends is a more promising avenue of inquiry.

Historical AA emissions are spatially and temporally heterogeneous, and can induce global (Deser, Phillips, et al., 2020; Hwang et al., 2013; Ming & Ramaswamy, 2009) and regional (Bollasina et al., 2011; Dong et al., 2014) precipitation changes. There are two modes to describe the historical AA emissions (Kang et al., 2021; Shi et al., 2022, 2023): (a) the aerosol increase mode, a global aerosol increase in the mid-20th century, inducing Northern Hemisphere cooling, and (b) the aerosol shift mode, an aerosol emission shift from the Western to the Eastern Hemisphere since 1980, inducing a negative PDV-like SST pattern. Idealized experiments with prescribed strong radiative forcings from aerosols (e.g., 5–10 times the observed emissions; Allen et al., 2020; Dow et al., 2021) and transient historical aerosols forcing (Allen & Zhao, 2022) show that AA, especially black carbon emissions from Asia, can induce a negative PDV-like pattern, weaken the AL, and influence precipitation over Western North America. Given the anticipated regional changes to aerosol emissions in the near future (Persad et al., 2022), understanding its influence on historical precipitation trends is key to develop more robust future projections.

In this study, we aim to quantify how much of the post-1980 SWUS precipitation change originates from internal or anthropogenically forced Pacific SST variability. Thereby, we attempt to extract as much information as possible from observations before turning to model simulations. We use a low-frequency component analysis (LFCA; Wills et al., 2018) to disentangle the forced and internal low-frequency Pacific SST variability and investigate how those SST patterns affect SWUS precipitation. Additionally, we assess the contributions from AA on SWUS precipitation with a set of idealized Community Earth System Model version 2 (CESM2) simulations.

2. Data Processing

We use observational and reanalysis data from 1940–2020 to understand Pacific SSTs low-frequency variability and its relationship to atmospheric circulation and precipitation. Monthly mean SST is taken from ERSSTv5 (Huang et al., 2017), monthly mean sea level pressure (SLP) is from European Centre for Medium-Range Weather Forecasts (ECMWF) Reanalysis version 5 (ERA5; Hersbach et al., 2020). Precipitation is taken from the Global Precipitation Climatology Center monthly precipitation data set with spatial resolution of 1° latitude/longitude (GPCC; Schneider et al., 2022). We remap observational and reanalysis data to CESM2's native nominal 1° latitude/longitude grid with a mass-conserving regridding scheme. We calculate the area-weighted average of precipitation over the SWUS using the domain 32.5–42°N, 102.5–125°W (land-only; red box in Figure 1).

We also use the 50-member CESM2 large ensemble with full radiative forcings (CESM2-LE; Rodgers et al., 2021) and a set of single forcing LEs with CESM2 (Simpson et al., 2023): (a) 15-member ensemble with anthropogenic aerosols only (AAER) and (b) 10-member ensemble with all forcings evolving, except AA is held fixed at 1920 values (xAAER). The 50 CESM2-LE members use the smoothed biomass burning (smbb) forcing, consistent with what is used in the single forcing experiments. We include a 2000-year pre-industrial simulation with fully coupled CESM2 (Danabasoglu et al., 2020) to estimate the distribution of precipitation trends from internal variability alone, calculated from overlapping 40-year periods. A 999-year pre-industrial simulation from CAM6 with fixed SST/sea ice seasonal cycle is also included to estimate the distribution of precipitation trends from internal atmospheric variability alone. The long-term drift in the pre-industrial simulations is removed following Lou et al. (2023). We define signal-to-noise ratio (S/N) as the ensemble mean divided by the ensemble spread (one standard deviation) to assess the significance of any simulated forced response.

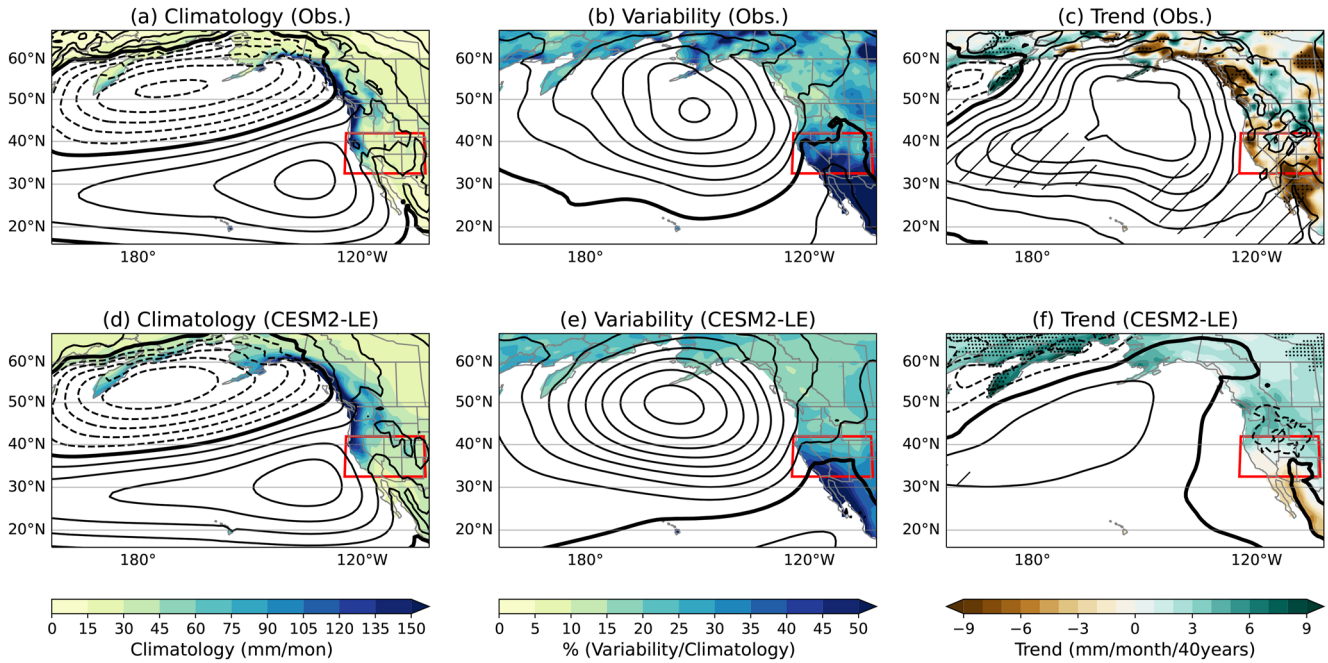

Figure 1. Observed 1980–2020 DJFMAM (a) climatology (sea level pressure (SLP) is relative to 1013.25 hPa; contour spacing 2 hPa; thick line indicates 0 hPa), (b) interannual variability (standard deviation after detrending; precipitation is given as percentage of climatology; contour spacing 0.5 hPa; thick line indicates 1 hPa), and (c) trend (contour spacing 0.5 hPa/40 years; thick line indicates 0 hPa/40 years; hatching/stippling indicates significant trend at 95% confidence level based on a *t*-test for SLP/precipitation). Panels (d)–(f) same as panels (a)–(c) but showing the ensemble mean of CESM2-LE. Hatching/stippling in (f) indicates a trend with S/N > 1 for SLP/precipitation.

LFCA is applied to monthly Pacific SSTs from ERSSTv5 (Wills et al., 2018) and an ensemble matrix from each model large ensemble (Wills et al., 2020) to obtain the dominant modes of variability on decadal and longer time scales. Previous studies demonstrated the effectiveness of LFCA for obtaining low-frequency variability in SST and sea ice (Dörr et al., 2023; Rollings & Merlis, 2021; Wills et al., 2020). Analogous to an Empirical Orthogonal Functions (EOFs) analysis, the goal of LFCA is to find the modes that maximize the low-frequency to total variance ratio (r_k). To do so, we apply EOF analyses and retain the minimum $\boldsymbol{N}$ EOFs that can explain more than 90% of the total variance in Pacific SST. Then, we project the Pacific SST, 10-year low-pass filtered with a Lanczos filter (Duchon, 1979), on the $\boldsymbol{N}$ EOFs and apply a singular value decomposition to obtain the low-frequency patterns and low-frequency components (LFPs/LFCs; analogous to EOFs/PCs) with the highest r_k. The mathematical basis of LFCA and discussion of its sensitivity to choices in low-pass filtering and number of EOFs retained are found in Wills et al. (2018).

We focus on the winter-spring precipitation and circulation defined as the December-May (DJFMAM) mean. To understand the teleconnections arising from the forced low-frequency Pacific SSTs, we apply a multivariate linear regression on DJFMAM precipitation and SLP with the normalized DJFMAM mean of $\boldsymbol{M}$ leading Pacific SST LFCs that capture forced signals during 1940–2020:

$$y(t) = \sum_{i=1}^{M} y_{\mathrm{LFC}_i}(t) + \varepsilon(t) = \sum_{i=1}^{M} \beta_{\mathrm{LFC}_i} \mathrm{LFC}_i(t) + \varepsilon(t) \quad (1)$$

Here, y is the variable of interest (e.g., precipitation, SLP), y_{LFC_i} is the reconstructed y as $\beta_{\mathrm{LFC}_i}\mathrm{LFC}_i$, where β_{LFC_i} is obtained by regressing the 10-year low-pass filtered y on the leading $\boldsymbol{M}$ LFCs. The first two modes capture physically meaningful and primarily forced responses (see also discussion in Wills et al., 2018). ε is the residual and is interpreted as internal variability and variability not associated with the forced Pacific SSTs. Using $\boldsymbol{M} = 2$ in the observations-based LFCs regression model yields an explained variance of 2%–55% and 0%–61% of the grid cell-level low-frequency variance of the low-pass filtered SWUS precipitation and North Pacific SLP (Figures S1b and S1d in Supporting Information S1). Due to the strong internal variability during winter-spring, the low-frequency signal regression captures only 0%–14% and 0%–6% of the *interannual* variance of the SWUS

precipitation and North Pacific SLP (Figures S1a and S1c in Supporting Information S1). Finally, we can decompose the observed trend (i.e., trend in y, noted as Δy) into different modes of Pacific SST low-frequency variability (i.e., trend in y_{LFC_i}) and the trend in ε as

$$\Delta y = \sum_{i=1}^{M} \Delta y_{\mathrm{LFC}_i} + \Delta\varepsilon = \sum_{i=1}^{M} \beta_{\mathrm{LFC}_i} \Delta \mathrm{LFC}_i + \Delta\varepsilon \quad (2)$$

3. Results

3.1. Overview of North Pacific and SWUS Winter-Spring Hydroclimate

Figure 1 shows the climatology, interannual variability, and trend of winter-spring SLP and precipitation during 1980–2020 from observations and CESM2-LE. The AL in the North Pacific transports moisture to the coastal SWUS and establishes a strong climatological precipitation gradient from the coast to the inland (Figure 1a). The highly variable AL leads to high relative precipitation variability over the SWUS, especially its coastal sector (Figure 1b). Generally, CESM2 reproduces these climatological patterns and their interannual variability (Figures 1d and 1e). CESM2 has a stronger climatological SLP gradient between the AL and the North Pacific Subtropical High and more precipitation in the central SWUS. The interannual variability of SLP in the North Pacific is overestimated in CESM2.

The observed 1980–2020 precipitation trend is negative over most of SWUS (Figure 1c), but insignificant due to the high variability in winter-spring. The ensemble mean of CESM2-LE indicates weaker trends for both SLP and SWUS precipitation, with S/N mostly <1 (Figure 1f). Of course, internal variability can contribute to a decadal trend in observation while it averages out in the CESM2-LE ensemble mean (Figures 1c and 1f).

3.2. Forced Low-Frequency Variability in Pacific SSTs

Applying LFCA to Pacific SSTs during 1940–2020, we obtain the leading two LFPs/LFCs with forced signals from ERSSTv5 and CESM2-LE (Figure 2). LFP1/LFC1 depicts a basin-wide warming trend, most likely representing the long-term warming signal from GHGs. LFP2/LFC2 shows a negative PDV-like pattern that is enhanced post-1980 and has been suggested to be forced by AA. To corroborate the hypothesized influence of external forcings on observed decadal Pacific SST variability in LFP1/LFC1 and LFP2/LFC2, we compare the leading two LFPs/LFCs from ERSSTv5 to the CESM2-simulated LFPs/LFCs, specifically the all-forcing CESM2-LE, AAER and xAAER ensembles (Figures 2 and 3).

The LFP1/LFC1 from ERSSTv5 and ensemble mean of CESM2-LE have a temporal correlation of 0.89 ($p < 0.01$, Figures 2e and 2g) during 1940–2020, while the pattern correlation is only 0.23 ($p < 0.01$, Figures 2a and 2c). The difference in spatial pattern arises from CESM2's lack of central North Pacific cooling and a more El Niño-like warming, something seen in most climate models (Lee et al., 2022; Seager, Cane, et al., 2019, 2022; Wills et al., 2022). LFP1/LFC1 from CESM2-LE resembles LFP1/LFC1 from xAAER (Figures 3a and 3d), implying that GHGs are the main driver of this mode. xAAER alone, however, cannot explain the 1940–1980 warming hiatus seen in ERSSTv5 and CESM2-LE; instead, the AA-driven basin-wide cooling contributes to this mid-20th century warming hiatus (Figures 3b and 3e). Regressing AAER's aerosol optical depth (AOD) onto AAER's LFC1 identifies the aerosol increase mode as the primary driver here (Figure S2 in Supporting Information S1). Here, the global increase mode features decreasing AOD over North America, differing from Shi et al. (2022) due to the choice of time period (1940–2020 vs. 1920–2080).

LFP2/LFC2 from ERSSTv5 and CESM2-LE ensemble mean have a temporal correlation of 0.47 ($p < 0.01$, Figures 2f and 2h) during 1940–2020 and a pattern correlation of 0.73 ($p < 0.01$, Figures 2b and 2d). The LFP2/LFC2 from CESM2-LE corresponds to the LFP2/LFC2 from AAER (Figures 3c and 3f), which is associated with the aerosol shift mode, corroborated by a regression of AOD onto LFC2 (Figure S2 in Supporting Information S1). LFP1/LFC1 in the fully coupled pre-industrial run and LFP2/LFC2 in xAAER are both PDV-like patterns (Figure S3 in Supporting Information S1), indicating internal variability itself can also generate this PDV pattern. However, the inclusion of AA forcing substantially increases the probability of a transition to a negative PDV-like pattern during 1980–2020 (Figure 4a). This supports the idea that the aerosol shift mode can influence SWUS precipitation trends through its potential to trigger a negative PDV.

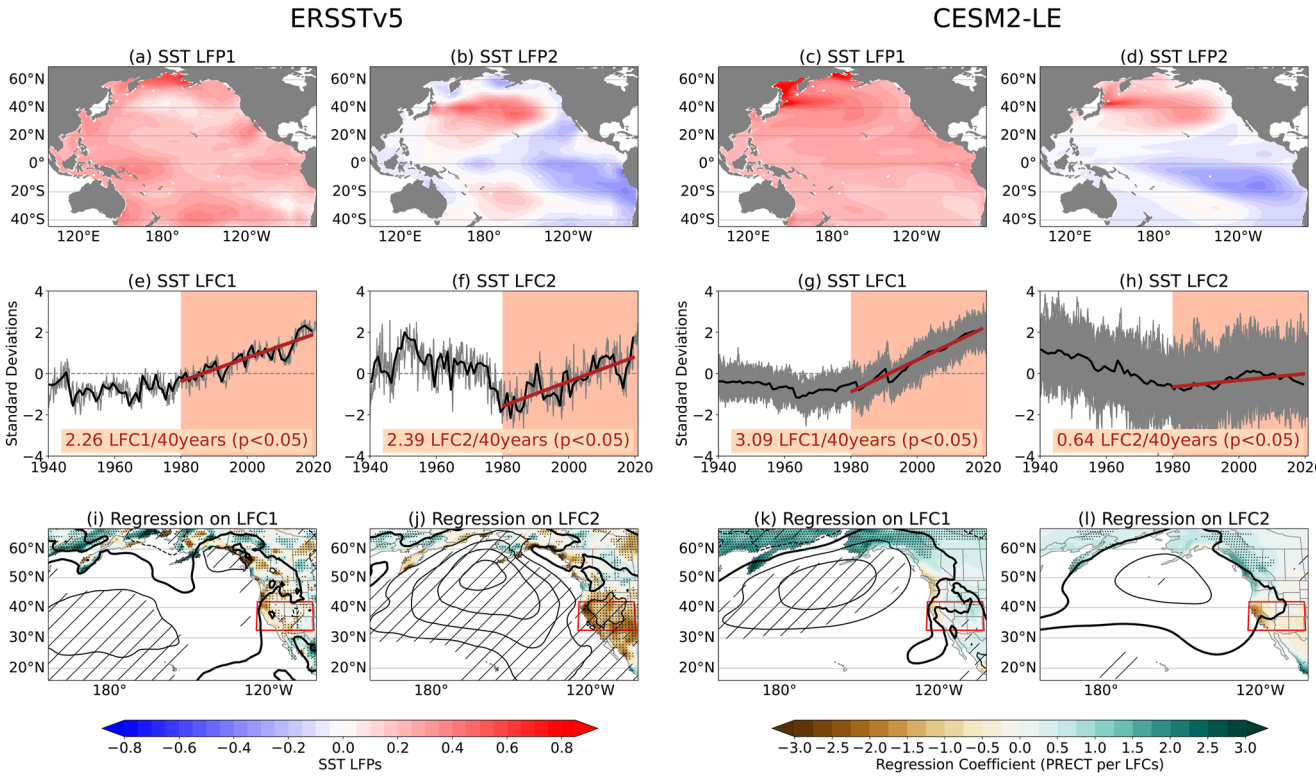

Figure 2. (a)–(d) LFPs, (e)–(h) monthly (gray) and DJFMAM mean (black) LFCs, and (i)–(l) regression maps of precipitation (mm/month) and sea level pressure (hPa) onto the LFCs over 1940–2020, based on ERSSTv5/GPCC/ERA5 (left two columns) and CESM2-LE (right two columns). Black lines in panels (e)–(h) are DJFMAM means of LFCs from ERSSTv5 and the ensemble mean of CESM2-LE; red lines and texts are linear trends of the black lines during 1980–2020. Hatching and stippling in panels (i)–(j) mark regression coefficients with 95% confidence level based on a *t*-test and (k)–(l) regression coefficients S/N > 1. Contour spacing in panels (i)–(l) is 0.15 hPa/LFCs with thick line indicating 0 hPa/LFCs.

3.3. Hydroclimate Teleconnection From Forced Pacific SST Low-Frequency Variability

Multivariate linear regressions of SLP and precipitation onto $\boldsymbol{M}$ LFCs illustrate how the forced Pacific SST low-frequency variability affects regional hydroclimate (Figures 2i–2l and Figures 3g–3i; $\boldsymbol{M}$ = 2 for observation, CESM2-LE, AAER and $\boldsymbol{M}$ = 1 for xAAER). The observed LFC1 (basin-wide warming) leads to a significant increase in North Pacific SLP and a decrease in SWUS precipitation (Figure 2i). The LFC1 regression in CESM2-LE shows a similar pattern, however, the SLP increase occurs further north in the Pacific and the precipitation decline is consequently also located further north along the coast, leaving the SWUS precipitation trend to be insignificant (Figures 2k). These discrepancies can be explained by the stronger LFP1 warming in CESM2-LE than observation (Figures 2a and 2c); a stronger North Pacific warming drives an SLP increase at higher latitudes (Choi et al., 2016), while the enhanced tropical Pacific warming in CESM2 and other models favors a more positive SWUS precipitation signals (Allen & Luptowitz, 2017).

Observed LFC2 significantly increases SLP over the North Pacific and decreases SWUS precipitation, consistent with the shift to a negative PDV. These patterns are well reproduced by CESM2-LE (Figure 2l) and the AAER ensemble (Figure 3i). However, the strengths of the regressions are weaker in CESM2 (both CESM2-LE and AAER) compared with observations (Figure 2j). It is possible that internal variability influences the regression coefficients (Figure 1e) or that CESM2 underestimates the externally forced circulation response (Scaife & Smith, 2018). Notably, the regression map of AAER has large areas of S/N > 1, while CESM2-LE does not (Figures 2l vs. 3i). This low S/N in CESM2-LE suggests that the AA forcing is offset by other forcings, such as GHGs (Dittus et al., 2021).

The observed LFCs regression maps are insensitive to conducting the LFCs-regression over 1940–2020 or 1980–2020 (Figure S4 in Supporting Information S1). In general, CESM2 captures the observed teleconnections from forced Pacific SST low-frequency variability. However, there are many regions outside of the SWUS where the

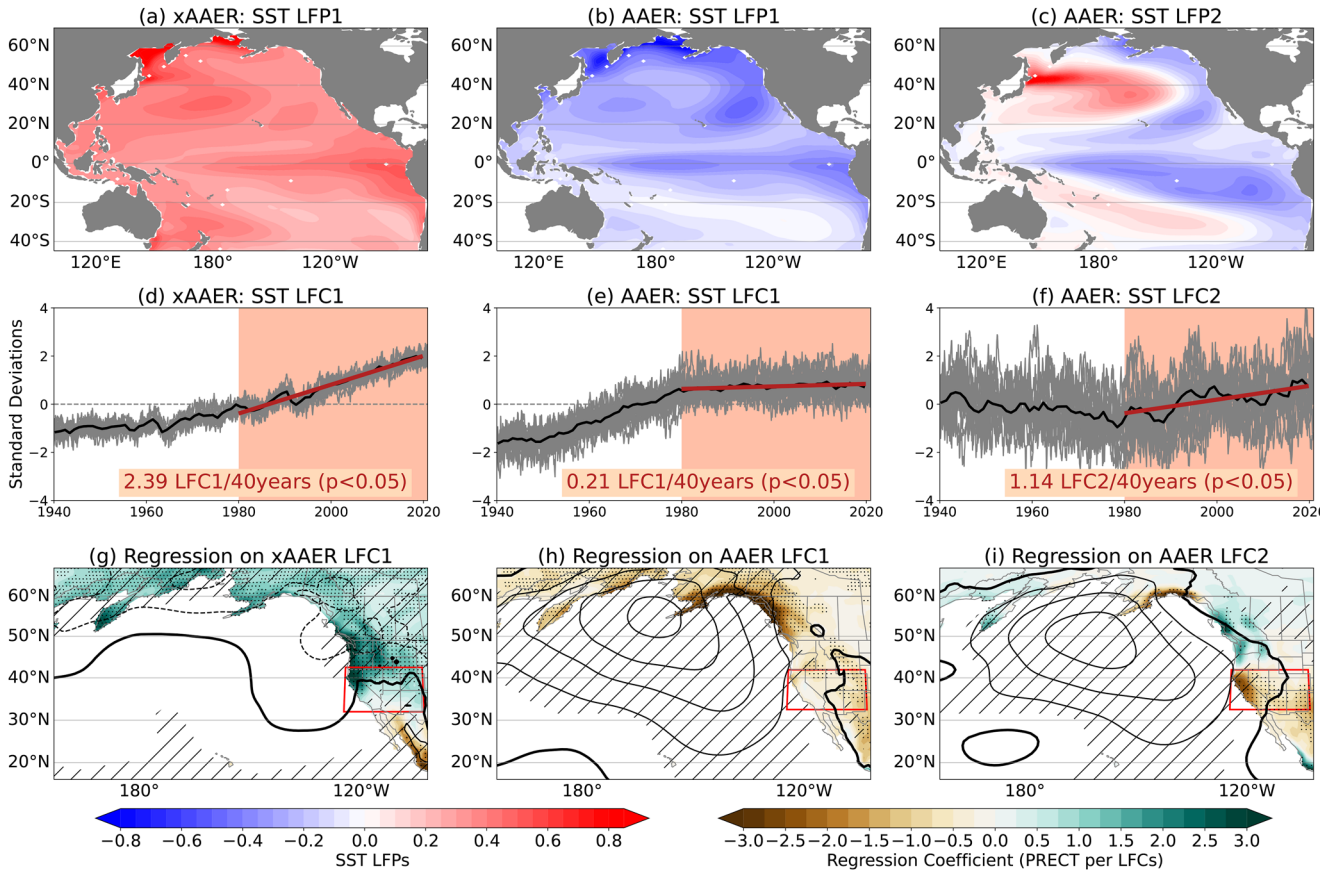

Figure 3. As in Figure 2 but panels (a), (d), (g) for the first mode from CESM2 xAAER and panels (b), (c), (d), (f), (h), (i) for the first two modes from AAER.

results from observations disagree with the smoother and more robust regression results from CESM2-LE. This can be either due to internal variability or true model-observation differences.

3.4. Observed Hydroclimate Trend Decomposition

We use Equation 2 to estimate the contributions from the forced Pacific SST low-frequency modes to the SWUS winter-spring precipitation (Figure 4b). The observed winter-spring precipitation decline (−2.8 mm/month/40 years) is primarily from LFC2 (−4.0 mm/month/40 years, 143% of the observed trend). The observed residual drives an increasing trend (2.1 mm/month/40 years, −75% of the observed trend), containing most of the interannual variability, including ENSO (Figure S5 in Supporting Information S1). Attributing all residuals is beyond the scope of this study, as we focus on the influence of the forced Pacific SST low-frequency variability.

The total forced trend estimated by CESM2-LE is a weak increasing trend, qualitatively following the wetting from xAAER with a competing drying from AAER. This again suggests the forced SWUS spring-winter precipitation in CESM2-LE leans toward xAAER's forced response. Decomposing the trends forced by Pacific low-frequency modes, the xAAER wetting is associated with the basin-wide warming (LFC1, 2.3 mm/month/40 years, −82% of the observed trend), while the AAER drying is from the negative PDV-like pattern (LFC2, -1.2 mm/month/40 years, 42% of the observed trend). This qualitatively agrees with observations, though the observed LFC2-related precipitation trend is an outlier in the context of LFC2-related trends from both CESM2-LE and AAER (Figure 4b). Note that the observed LFC2-related trend is inevitably a mix of AA-forced response and internal PDV variability. To what extent, quantitatively, the observed LFC2 is forced remains unclear. 40-year winter-spring SWUS precipitation trends from CESM2's pre-industrial simulations can create a wide range of trends, even from atmospheric internal variability alone (Figure 4b green and brown distribution). However, it is evident that the AA-forced response shifts the total forced response toward the observed SWUS

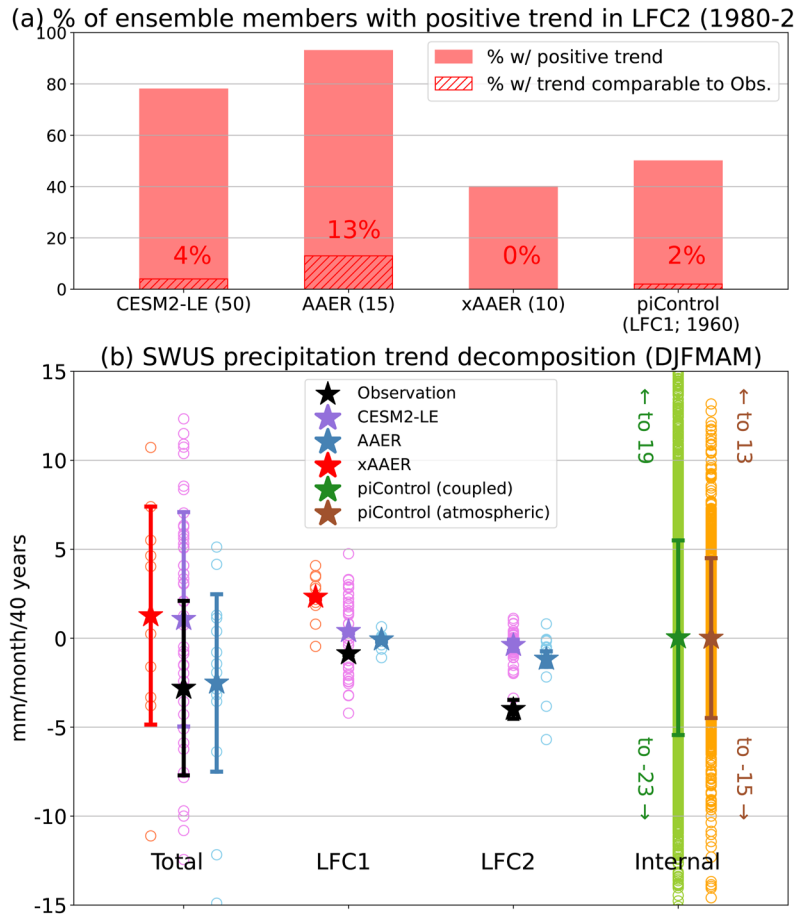

Figure 4. (a) Percentage of Community Earth System Model version 2 (CESM2) ensemble members with a positive 1980–2020 DJFMAM LFC2 trend (red bars; hatched if model trend ≥ observed trend) (see Figure 2f) for CESM2-LE (50 ensemble members), AAER (15), and xAAER (10) and pre-industrial simulation (1960; LFC1). (b) Decomposition of observed DJFMAM SWUS precipitation trend with LFCs. Error bars around observations (black) are 1 standard deviation of its trend. Stars, ranges, and dots for CESM2 represent ensemble mean trends, ensemble mean standard deviation of trends, and individual ensemble members.

drying associated with a negative PDV shift. We speculate that the AA-forced response acts qualitatively similar in reality.

The observed LFC2 trend magnitude is rare but not unseen in CESM2 (Figure 4a), yet CESM2-LE does not produce the corresponding precipitation trends (Figure S6 in Supporting Information S1). However, the AAER ensemble appears to have the right relationship between trends in LFC2 and SWUS precipitation, producing PDV-related SWUS drying more comparable to the observations than CESM2-LE (Figure S6 in Supporting Information S1). This suggests that CESM2 in general reproduces the aerosol response that favors the observed SWUS drying, but that it is too weak compared to other forcings (see also Dittus et al., 2021).

4. Discussion and Conclusion

Using a combination of LFCA and multivariate linear regression, we find the observed winter-spring SWUS precipitation decline since 1980 to be primarily driven by a negative PDV-like pattern, consistent with previous studies (Delworth et al., 2015; Lehner et al., 2018; Seager & Hoerling, 2014; Seager & Ting, 2017). While these trends were often attributed to internal variability, we show evidence with CESM2 that they are, in part, a forced response to anthropogenic aerosols (AA; up to 42% of the observed precipitation trend). Specifically, the AA-driven negative PDV-like pattern originates from the post-1980 shift of aerosol emissions from the Western to the Eastern Hemisphere, which has been suggested to be conducive to SWUS precipitation declines (Allen & Zhao, 2022; Allen et al., 2020).

Our estimate of SWUS precipitation decrease associated with the PDV shift in observation is stronger than in CESM2 simulations. It remains unclear whether this is a sampling problem or whether CESM2 simulates a too-weak AA-forced response. In fact, whether parts of the decadal Pacific SST variability are forced by AA (Qin et al., 2020; Smith et al., 2016; Takahashi & Watanabe, 2016; Wills et al., 2018) or not (Oudar et al., 2018) is still debated given the small S/N from aerosols and the potential inability of climate models to simulate the correct strength of aerosol-caused cooling (Dittus et al., 2021; Oudar et al., 2018). Recent concerns about whether models correctly represent the S/N of the real world, leading to a signal-to-noise paradox in climate models (Scaife & Smith, 2018), could be at play in the North Pacific as well. PDV involves several processes and patterns (Newman et al., 2016), so it is challenging to separate the AA-induced PDV shift from the pure internally driven PDV that it projects onto. Large ensembles are thus clearly necessary to separate forced responses from internal variability (Deser, Lehner, et al., 2020), and to study regional aerosol responses.

The residual in our study is indeed large and contains ENSO and other drivers of SWUS precipitation, including intrinsic atmospheric variability (Lehner & Deser, 2023), teleconnections from other ocean basins (McGregor et al., 2014; Seager et al., 2005), and local drivers of precipitation (e.g., land-atmospheric interactions; Dirmeyer et al., 2013). The relative importance of these sources of variability remains unknown and may require additional idealized model simulations to disentangle. CESM2 shows a balance between the effects of aerosol forcing (drying) and everything-but-aerosol forcing (wetting) on SWUS precipitation, a balance that leans toward the xAAER forced response but is clearly sensitive to the exact location of the North Pacific SLP response pattern. Such counteracting effects, and their model dependency, may explain why previous studies found an insignificant net anthropogenically forced SWUS precipitation trend (Delworth et al., 2015; Lehner et al., 2018; Seager, Osborn, et al., 2019). Given the sizable model uncertainty in regional aerosol forcing and hydroclimate response to it (Lehner & Coats, 2021), future work will need to investigate the across-model robustness of our CESM2-based results.

As temperature is projected to increase further in the future, the main uncertainty around SWUS drought occurrence is precipitation. Here we demonstrate that up to 42% of the observed winter-spring precipitation trend since 1980 is driven by AA within CESM2. An important implication is that as aerosol emissions continue to change, so will their influence on regional precipitation via SSTs. This is consistent with the hypothesis that changes in the zonal gradient of tropical Pacific SST so far mimic a tug-of-war between GHGs and aerosols that might reverse and shift toward Eastern equatorial warming as aerosol emissions subside and GHGs continue to increase (Heede & Fedorov, 2021). Consequently, reducing uncertainty in future regional precipitation trends depends on a better understanding of the influences from both GHGs and aerosol forcings.

Data Availability Statement

The information to access CESM2-LE and single forcing simulations can be found https://www.cesm.ucar.edu/community-projects/lens2/data-sets; Research Data Archive (RDA) at NCAR provides access to ERSSTv5 (Huang et al., 2017; National Centers for Environmental Information/NESDIS/NOAA/U.S. Department of Commerce, 2019) and ERA5 (European Centre for Medium-Range Weather Forecasts, 2019; Hersbach et al., 2020); GPCC is accessed through Schneider et al. (2022). Codes to perform LFCA can be found at https://github.com/rcjwills/lfca and codes to generate the results in this study are available at Kuo (2023).

Acknowledgments
We thank two anonymous reviewers for constructive comments, and Robert J. Wills for helpful feedback on an earlier version of the manuscript. The authors were supported by NOAA MAPP award NA21OAR4310349. FL acknowledges support from the U.S. Department of Energy, Office of Science, Office of Biological & Environmental Research (BER), Regional and Global Model Analysis (RGMA) component of the Earth and Environmental System Modeling Program under Award Number DE-SC0022070 and National Science Foundation (NSF) IA 1947282. The National Center for Atmospheric Research (NCAR) is sponsored by NSF. We thank the data centers who provide observational data, and NCAR and IBS Center for Climate Physics for making available the CESM2-LE and single forcing simulations.

References

Allen, R. J., Lamarque, J., Watson-Parris, D., & Olivié, D. (2020). Assessing California wintertime precipitation responses to various climate drivers. *Journal of Geophysical Research: Atmospheres*, *125*(12), e2019JD031736. https://doi.org/10.1029/2019JD031736

Allen, R. J., & Luptowitz, R. (2017). El Niño-like teleconnection increases California precipitation in response to warming. *Nature Communications*, *8*(1), 16055. https://doi.org/10.1038/ncomms16055

Allen, R. J., & Zhao, X. (2022). Anthropogenic aerosol impacts on Pacific Coast precipitation in CMIP6 models. *Environmental Research: Climate*, *1*, 015005. https://doi.org/10.1088/2752-5295/ac7d68

Bollasina, M. A., Ming, Y., & Ramaswamy, V. (2011). Anthropogenic aerosols and the weakening of the south Asian summer monsoon. *Science*, *334*(6055), 502–505. https://doi.org/10.1126/science.1204994

Bonfils, C. J. W., Santer, B. D., Fyfe, J. C., Marvel, K., Phillips, T. J., & Zimmerman, S. R. H. (2020). Human influence on joint changes in temperature, rainfall and continental aridity. *Nature Climate Change*, *10*(8), 726–731. https://doi.org/10.1038/s41558-020-0821-1

Chavez, F. P., Ryan, J., Lluch-Cota, S. E., & Ñiquen, C. M. (2003). From anchovies to sardines and back: Multidecadal change in the Pacific Ocean. *Science*, *299*(5604), 217–221. https://doi.org/10.1126/science.1075880

Choi, J., Lu, J., Son, S., Frierson, D. M. W., & Yoon, J. (2016). Uncertainty in future projections of the North Pacific subtropical high and its implication for California winter precipitation change. *Journal of Geophysical Research: Atmospheres*, *121*(2), 795–806. https://doi.org/10.1002/2015JD023858

Danabasoglu, G., Lamarque, J., Bacmeister, J., Bailey, D. A., DuVivier, A. K., Edwards, J., et al. (2020). The community Earth system model version 2 (CESM2). *Journal of Advances in Modeling Earth Systems*, *12*. https://doi.org/10.1029/2019MS001916

Delworth, T. L., Zeng, F., Rosati, A., Vecchi, G. A., & Wittenberg, A. T. (2015). A link between the hiatus in global warming and North American drought. *Journal of Climate*, *28*(9), 3834–3845. https://doi.org/10.1175/JCLI-D-14-00616.1

Deser, C., Lehner, F., Rodgers, K. B., Ault, T., Delworth, T. L., DiNezio, P. N., et al. (2020). Insights from Earth system model initial-condition large ensembles and future prospects. *Nature Climate Change*, *10*(4), 277–286. https://doi.org/10.1038/s41558-020-0731-2

Deser, C., Phillips, A. S., Simpson, I. R., Rosenbloom, N., Coleman, D., Lehner, F., et al. (2020). Isolating the evolving contributions of anthropogenic aerosols and greenhouse gases: A new CESM1 large ensemble community resource. *Journal of Climate*, *33*(18), 7835–7858. https://doi.org/10.1175/JCLI-D-20-0123.1

Dirmeyer, P. A., Jin, Y., Singh, B., & Yan, X. (2013). Trends in land–atmosphere interactions from CMIP5 simulations. *Journal of Hydrometeorology*, *14*(3), 829–849. https://doi.org/10.1175/JHM-D-12-0107.1

Dittus, A. J., Hawkins, E., Robson, J. I., Smith, D. M., & Wilcox, L. J. (2021). Drivers of recent North Pacific decadal variability: The role of aerosol forcing. *Earth's Future*, *9*(12), e2021EF002249. https://doi.org/10.1029/2021EF002249

Dong, B., Sutton, R. T., Highwood, E., & Wilcox, L. (2014). The impacts of European and Asian anthropogenic sulfur dioxide emissions on Sahel rainfall. *Journal of Climate*, *27*(18), 7000–7017. https://doi.org/10.1175/JCLI-D-13-00769.1

Dörr, J. S., Bonan, D. B., Årthun, M., Svendsen, L., & Wills, R. C. J. (2023). *Forced and internal components of observed Arctic sea-ice changes*. Sea ice/Climate Interactions.

Dow, W. J., Maycock, A. C., Lofverstrom, M., & Smith, C. J. (2021). The effect of anthropogenic aerosols on the Aleutian low. *Journal of Climate*, *34*(5), 1725–1741. https://doi.org/10.1175/JCLI-D-20-0423.1

Duchon, C. (1979). Lanczos filtering in one and two dimensions (pp. 1016–1022). https://doi.org/10.1175/1520-0450(1979)018<1016:LFIOAT>2.0.CO;2

European Centre for Medium-Range Weather Forecasts. (2019). ERA5 reanalysis (monthly mean 0.25 degree latitude-longitude grid) [Dataset]. Research Data Archive at the National Center for Atmospheric Research, Computational and Information Systems Laboratory. https://doi.org/10.5065/P8GT-0R61

Gleick, P. H. (2010). Roadmap for sustainable water resources in southwestern North America. *Proceedings of the National Academy of Sciences of the United States of America*, *107*(50), 21300–21305. https://doi.org/10.1073/pnas.1005473107

Heede, U. K., & Fedorov, A. V. (2021). Eastern equatorial Pacific warming delayed by aerosols and thermostat response to CO_2 increase. *Nature Climate Change*, *11*(8), 696–703. https://doi.org/10.1038/s41558-021-01101-x

Hersbach, H., Bell, B., Berrisford, P., Hirahara, S., Horányi, A., Muñoz-Sabater, J., et al. (2020). The ERA5 global reanalysis. *Quarterly Journal of the Royal Meteorological Society*, *146*(730), 1999–2049. https://doi.org/10.1002/qj.3803

Horel, J., & Wallace, J. (1981). Planetary-scale atmospheric phenomena associated with the southern oscillation (pp. 813–829). https://doi.org/10.1175/1520-0493(1981)109<0813:PSAPAW>2.0.CO;2

Huang, B., Thorne, P. W., Banzon, V. F., Boyer, T., Chepurin, G., Lawrimore, J. H., et al. (2017). Extended reconstructed Sea Surface temperature, version 5 (ERSSTv5): Upgrades, validations, and intercomparisons. *Journal of Climate*, *30*(20), 8179–8205. https://doi.org/10.1175/JCLI-D-16-0836.1

Hwang, Y., Frierson, D. M. W., & Kang, S. M. (2013). Anthropogenic sulfate aerosol and the southward shift of tropical precipitation in the late 20th century. *Geophysical Research Letters*, *40*(11), 2845–2850. https://doi.org/10.1002/grl.50502

Kang, S. M., Xie, S.-P., Deser, C., & Xiang, B. (2021). Zonal mean and shift modes of historical climate response to evolving aerosol distribution. *Science Bulletin*, *66*(23), 2405–2411. https://doi.org/10.1016/j.scib.2021.07.013

Kuo, Y.-N. (2023). ynkuo/kuo23_lfca_swusPtrd: July 11, 2023 Release (Version 1.0.0) [Software]. Zenodo. https://doi.org/10.5281/zenodo.8136496

Lee, S., L'Heureux, M., Wittenberg, A. T., Seager, R., O'Gorman, P. A., & Johnson, N. C. (2022). On the future zonal contrasts of equatorial Pacific climate: Perspectives from Observations, Simulations, and Theories. *npj Climate and Atmospheric Science*, *5*(1), 82. https://doi.org/10.1038/s41612-022-00301-2

Lehner, F., & Coats, S. (2021). Does regional hydroclimate change scale linearly with global warming? *Geophysical Research Letters*, *48*(23). https://doi.org/10.1029/2021GL095127

Lehner, F., & Deser, C. (2023). Origin, importance, and predictive limits of internal climate variability. *Environmental Research: Climate*, *2*, 023001. https://doi.org/10.1088/2752-5295/accf30

Lehner, F., Deser, C., Simpson, I. R., & Terray, L. (2018). Attributing the U.S. Southwest's recent shift into drier conditions. *Geophysical Research Letters*, *45*(12), 6251–6261. https://doi.org/10.1029/2018GL078312

Lin, Y.-H., Hipps, L. E., Wang, S.-Y. S., & Yoon, J.-H. (2017). Empirical and modeling analyses of the circulation influences on California precipitation deficits: California drought variation. *Atmospheric Science Letters*, *18*(1), 19–28. https://doi.org/10.1002/asl.719

Lou, J., Newman, M., & Hoell, A. (2023). Multi-decadal variation of ENSO forecast skill since the late 1800s. *npj Climate and Atmospheric Science*, *6*(1), 89. https://doi.org/10.1038/s41612-023-00417-z

Marvel, K., Cook, B. I., Bonfils, C. J. W., Durack, P. J., Smerdon, J. E., & Williams, A. P. (2019). Twentieth-century hydroclimate changes consistent with human influence. *Nature*, *569*(7754), 59–65. https://doi.org/10.1038/s41586-019-1149-8

McGregor, S., Timmermann, A., Stuecker, M. F., England, M. H., Merrifield, M., Jin, F.-F., & Chikamoto, Y. (2014). Recent Walker circulation strengthening and Pacific cooling amplified by Atlantic warming. *Nature Climate Change*, *4*(10), 888–892. https://doi.org/10.1038/nclimate2330

McKinnon, K. A., & Deser, C. (2021). The inherent uncertainty of precipitation variability, trends, and extremes due to internal variability, with implications for Western US water resources. *Journal of Climate*, 1–46. https://doi.org/10.1175/JCLI-D-21-0251.1

Ming, Y., & Ramaswamy, V. (2009). Nonlinear climate and hydrological responses to aerosol effects. *Journal of Climate*, *22*(6), 1329–1339. https://doi.org/10.1175/2008JCLI2362.1

National Centers for Environmental Information/NESDIS/NOAA/U.S. Department of Commerce. (2019). NOAA NCEI extended reconstructed Sea Surface temperature [Dataset]. Research Data Archive at the National Center for Atmospheric Research, Computational and Information Systems Laboratory. https://doi.org/10.5065/JZ08-3W17

Newman, M., Alexander, M. A., Ault, T. R., Cobb, K. M., Deser, C., Di Lorenzo, E., et al. (2016). The Pacific decadal oscillation, revisited. *Journal of Climate*, *29*(12), 4399–4427. https://doi.org/10.1175/JCLI-D-15-0508.1

Oudar, T., Kushner, P. J., Fyfe, J. C., & Sigmond, M. (2018). No impact of anthropogenic aerosols on early 21st century global temperature trends in a large initial-condition ensemble. *Geophysical Research Letters*, *45*(17), 9245–9252. https://doi.org/10.1029/2018GL078841

Persad, G. G., Samset, B. H., & Wilcox, L. J. (2022). Aerosols must be part of climate risk assessments.

Pierce, D. W., Cayan, D. R., Das, T., Maurer, E. P., Miller, N. L., Bao, Y., et al. (2013). The key role of heavy precipitation events in climate model disagreements of future annual precipitation changes in California. *Journal of Climate*, *26*(16), 5879–5896. https://doi.org/10.1175/JCLI-D-12-00766.1

Polade, S. D., Gershunov, A., Cayan, D. R., Dettinger, M. D., & Pierce, D. W. (2017). Precipitation in a warming world: Assessing projected hydro-climate changes in California and other Mediterranean climate regions. *Scientific Reports*, *7*(1), 10783. https://doi.org/10.1038/s41598-017-11285-y

Qin, M., Dai, A., & Hua, W. (2020). Aerosol-forced multidecadal variations across all ocean basins in models and observations since 1920. *Science Advances*, *6*(29), eabb0425. https://doi.org/10.1126/sciadv.abb0425

Rodgers, K. B., Lee, S. S., Rosenbloom, N., Timmermann, A., Danabasoglu, G., Deser, C., et al. (2021). Ubiquity of human-induced changes in climate variability. *Earth System Dynamics*, *12*(4), 1393–1411. https://doi.org/10.5194/esd-12-1393-2021

Rollings, M., & Merlis, T. M. (2021). The observed relationship between Pacific SST variability and Hadley cell extent trends in reanalyses. *Journal of Climate*, *34*(7), 2511–2527. https://doi.org/10.1175/JCLI-D-20-0410.1

Samset, B. H. (2018). How cleaner air changes the climate. *Science*, *360*(6385), 148–150. https://doi.org/10.1126/science.aat1723

Scaife, A. A., & Smith, D. (2018). A signal-to-noise paradox in climate science. *npj Climate and Atmospheric Science*, *1*, 28. https://doi.org/10.1038/s41612-018-0038-4

Schneider, U., Hänsel, S., Finger, P., Rustemeier, E., & Ziese, M. (2022). GPCC full data monthly product version 2022 at 1.0°: Monthly land-surface precipitation from rain-Gauges built on GTS-based and historical data [Dataset]. https://doi.org/10.5676/DWD_GPCC/FD_M_V2022_100

Seager, R., Cane, M., Henderson, N., Lee, D.-E., Abernathey, R., & Zhang, H. (2019). Strengthening tropical Pacific zonal sea surface temperature gradient consistent with rising greenhouse gases. *Nature Climate Change*, *9*(7), 517–522. https://doi.org/10.1038/s41558-019-0505-x

Seager, R., Henderson, N., & Cane, M. (2022). Persistent discrepancies between observed and modeled trends in the tropical Pacific Ocean. *Journal of Climate*, *35*(14), 4571–4584. https://doi.org/10.1175/JCLI-D-21-0648.1

Seager, R., & Hoerling, M. (2014). Atmosphere and ocean origins of North American droughts. *Journal of Climate*, *27*(12), 4581–4606. https://doi.org/10.1175/JCLI-D-13-00329.1

Seager, R., Kushnir, Y., Herweijer, C., Naik, N., & Velez, J. (2005). Modeling of tropical forcing of persistent droughts and pluvials over Western North America: 1856–2000. *Journal of Climate*, *18*(19), 4065–4088. https://doi.org/10.1175/JCLI3522.1

Seager, R., Osborn, T. J., Kushnir, Y., Simpson, I. R., Nakamura, J., & Liu, H. (2019). Climate variability and change of mediterranean-type climates. *Journal of Climate*, *32*(10), 2887–2915. https://doi.org/10.1175/JCLI-D-18-0472.1

Seager, R., & Ting, M. (2017). Decadal drought variability over North America: Mechanisms and predictability. *Current Climate Change Reports*, *3*(2), 141–149. https://doi.org/10.1007/s40641-017-0062-1

Shi, J., Kwon, Y., & Wijffels, S. E. (2023). Subsurface Ocean temperature responses to the anthropogenic aerosol forcing in the North Pacific. *Geophysical Research Letters*, *50*(2), e2022GL101035. https://doi.org/10.1029/2022GL101035

Shi, J.-R., Kwon, Y.-O., & Wijffels, S. E. (2022). Two distinct modes of climate responses to the anthropogenic aerosol forcing changes. *Journal of Climate*, *35*(11), 3445–3457. https://doi.org/10.1175/JCLI-D-21-0656.1

Simpson, I. R., Rosenbloom, N., Danabasoglu, G., Deser, C., Yeager, S. G., McCluskey, C. S., et al. (2023). The CESM2 single-forcing large ensemble and comparison to CESM1: Implications for experimental design. *Journal of Climate*, *36*(17), 5687–5711. https://doi.org/10.1175/JCLI-D-22-0666.1

Smith, D. M., Booth, B. B. B., Dunstone, N. J., Eade, R., Hermanson, L., Jones, G. S., et al. (2016). Role of volcanic and anthropogenic aerosols in the recent global surface warming slowdown. *Nature Climate Change*, *6*(10), 936–940. https://doi.org/10.1038/nclimate3058

Takahashi, C., & Watanabe, M. (2016). Pacific trade winds accelerated by aerosol forcing over the past two decades. *Nature Climate Change*, *6*(8), 768–772. https://doi.org/10.1038/nclimate2996

Ukkola, A. M., De Kauwe, M. G., Roderick, M. L., Abramowitz, G., & Pitman, A. J. (2020). Robust future changes in meteorological drought in CMIP6 projections despite uncertainty in precipitation. *Geophysical Research Letters*, *47*(11), e2020GL087820. https://doi.org/10.1029/2020GL087820

Williams, A. P., Cook, B. I., & Smerdon, J. E. (2022). Rapid intensification of the emerging southwestern North American megadrought in 2020–2021. *Nature Climate Change*, *12*(3), 232–234. https://doi.org/10.1038/s41558-022-01290-z

Williams, A. P., Cook, E. R., Smerdon, J. E., Cook, B. I., Abatzoglou, J. T., Bolles, K., et al. (2020). Large contribution from anthropogenic warming to an emerging North American megadrought. *Science*, *368*(6488), 314–318. https://doi.org/10.1126/science.aaz9600

Wills, R. C., Schneider, T., Wallace, J. M., Battisti, D. S., & Hartmann, D. L. (2018). Disentangling global warming, multidecadal variability, and El Niño in Pacific temperatures. *Geophysical Research Letters*, *45*(5), 2487–2496. https://doi.org/10.1002/2017GL076327

Wills, R. C. J., Battisti, D. S., Armour, K. C., Schneider, T., & Deser, C. (2020). Pattern recognition methods to separate forced responses from internal variability in climate model ensembles and observations. *Journal of Climate*, *33*(20), 8693–8719. https://doi.org/10.1175/JCLI-D-19-0855.1

Wills, R. C. J., Dong, Y., Proistosecu, C., Armour, K. C., & Battisti, D. S. (2022). Systematic climate model biases in the large-scale patterns of recent sea-surface temperature and sea-level pressure change. *Geophysical Research Letters*, *49*(17), e2022GL100011. https://doi.org/10.1029/2022GL100011

Zhang, H., Seager, R., He, J., Diao, H., & Pascale, S. (2021). Quantifying atmosphere and ocean origins of North American precipitation variability. *Climate Dynamics*, *56*(11–12), 4051–4074. https://doi.org/10.1007/s00382-021-05685-0

Zhao, A., Stevenson, D. S., & Bollasina, M. A. (2019). Climate forcing and response to greenhouse gases, aerosols, and ozone in CESM1. *Journal of Geophysical Research: Atmospheres*, *124*(24), 13876–13894. https://doi.org/10.1029/2019JD030769